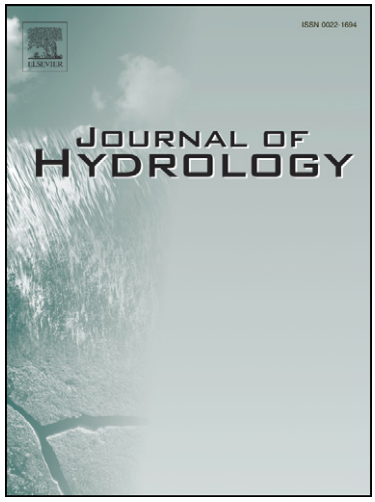

A Semi-Empirical Inversion Model for Assessing Surface Soil Moisture using AMSR-E Brightness Temperatures

Xiuzhi Chen, Shuisen Chen, Ruofei Zhong, Yongxian Su, Jishan Liao, Dan Li, Liusheng Han, Jianming Huang, Xia Li

PII: S0022-1694(12)00398-8
DOI: http://dx.doi.org/10.1016/j.jhydrol.2012.05.022
Reference: HYDROL 18240

To appear in: *Journal of Hydrology*

Received Date: 31 December 2011
Revised Date: 16 April 2012
Accepted Date: 9 May 2012

Please cite this article as: Chen, X., Chen, S., Zhong, R., Su, Y., Liao, J., Li, D., Han, L., Huang, J., Li, X., A Semi-Empirical Inversion Model for Assessing Surface Soil Moisture using AMSR-E Brightness Temperatures, *Journal of Hydrology* (2012), doi: http://dx.doi.org/10.1016/j.jhydrol.2012.05.022

A Semi-Empirical Inversion Model for Assessing Surface Soil Moisture using AMSR-E Brightness Temperatures

Xiuzhi Chen [a, c,d#], Shuisen Chen [a,b,f#], Ruofei Zhong[b*], Yongxian Su [a,c,d], Jishan Liao[e], Dan Li [a, c,d], Liusheng Han [a,c,d], Jianming Huang[a], Xia Li [g]

[a] Open Laboratory of Geo-spatial Information Technology and Application of Guangdong Province, Guangzhou Institute of Geography, Guangzhou 510070, China [#] Co-first authors

[b] Capital Normal University Key Lab of 3D Information Acquisition and Application, MOE, Beijing 100037, China [*]Corresponding author, Email: zrfgis@263.net

[c] Guangzhou Institute of Geochemistry, CAS, Guangzhou 510070, China

[d] Graduate School of Chinese Academy of Sciences, Beijing 100049, China

[e] State Key Lab of Remote Sensing Science, Jointly Sponsored by Institute of Remote Sensing Applications, Chinese Academy of Sciences, and Beijing Normal University, Beijing 100101, China

[f] College of Earth, Ocean, and Atmospheric Sciences, Oregon State University, Corvallis, OR 97331-5503, USA

[g] Department of Insurance, Guangdong University of Finance, Guangzhou 510521, China

[h] School of Geography and Planning, Sun Yat-sen University, Guangzhou 510275, China

Abstract: In 2004-2005, 2007 and 2009, three major drought disasters occurred in Guangdong Province of southern China, which caused serious economic losses. Hence, it has recently become an important research subject in China to monitor surface soil moisture (SSM) and the drought disaster quickly and accurately. SSM is an effective indicator for characterizing the degree of

drought. First, using the brightness temperatures (T_b) of the Advanced Microwave Scanning Radiometer on the EOS Aqua Satellite (AMSR-E), a modified surface roughness index was developed to map the land surface roughness. Then by combining microwave polarization difference indices (MPDI)-based vegetation cover classification and the modified surface roughness index, a simple semi-empirical model of SSM was derived from the passive microwave radiative transfer equation using AMSR-E C-band T_b and observed surface soil temperature (T_s). The model was inverted to calculate SSM. The results show the ability to discriminate over a broad range of SSM (7%~73%) with an accuracy of 2.11% in bare ground and flat areas (R^2 =0.87), 2.89% in sparse vegetation and flat surface areas (R^2=0.85), about 6%~9% in dense vegetation areas and rough surface areas ($0.80 \leq R^2 \leq 0.83$). The simulation results were also validated using in-situ SSM data (R^2=0.87, RMSE=6.36%). Time series mapping of SSM from AMSR-E imageries further demonstrated that the presented method was effective to detect the initiation, duration and recovery of the drought events.

Keywords: surface soil moisture (SSM); Semi-Empirical model; brightness temperature (T_b); AMSR-E; passive microwave remote sensing; drought disaster; south China

1. Introduction

Surface soil moisture (SSM) is not only an important variable used to describe water and energy exchanges at the land surface and atmosphere interface (Wigneron et al., 2003); it is also an effective indicator for characterizing the degree of drought. In 2004, 2007 and 2009, three disastrous droughts occurred in Guangdong Province of southern China, causing serious economic losses (about 30 billion Yuan, http://www.chinadaily.com.cn/). Since the 1990s, the total economic losses caused by drought disasters have been equivalent to 1.1 percent of China's average annual

gross domestic product (about 324 billion Yuan, http://www.chinadaily.com.cn/). As a result there is a requirement for the timely estimation of regional SSM information on a large scale for drought disaster emergency management. Passive microwave remotely sensed data has great potential for providing estimates of SSM with good temporal coverage on a daily basis and on a regional scale (Wigneron et al., 2003). Here we develop an improved SSM retrieval model and demonstrate its utility to monitor the drought condition using passive microwave remote sensing data.

Passive microwave remote sensing data has been used to retrieve SSM for almost 35 years. Numerous studies indicated a strong relationship between the microwave brightness temperature (T_b) and SSM content (Eagleman and Lin, 1976; Schmugge et al., 1988; Wang et al., 1989; Wang et al., 1990; Jackson et al., 1995; Jackson et al., 1997; Schmugge, 1998; Jackson et al., 1999; Uitdewilligen et al., 2003). Ulaby et al. (1981) and Liebe (1989) recommended using absorption lines at 6.6GHz because of the high sensitivity to atmospheric water vapor at frequencies higher than 10.7 GHz. Building on this, Owe et al., (2008) used C band (6.6GHz) and L band (10.7 GHz) passive measurements to retrieve SSM from space. But microwave emissions are also strongly affected by land surface properties (such as soil physical properties, vegetation characters and surface soil temperature T_s), including C- and L-band emissions that were chosen because they are less sensitive to atmospheric and tenuous clouds emissions (Owe et al., 2001). So SSM retrieval algorithms from passive microwave data have to account for the effects of such land surface properties. Many studies have been conducted to develop a method for compensating for the errors caused by soil texture, soil roughness, soil temperature and land surface vegetation cover condition (Dobson et al., 1985; Hallikainen et al., 1985; Choudhury et al., 1982; Choudhury, 1987;

Jackson and Schmugge, 1989; Schmugge and Jackson, 1992; Chanzy and Wigneron, 2000; Uitdewilligen et al., 2003). Lacava et al. (2005) first eliminated the surface roughness and vegetation water content affects which impact the SSM retrieval accuracy from AMSR-E and then simulated the global SSM condition using soil wetness variation index (SWVI). Mallick et al. (2009) established a soil wetness index from surface soil temperature (T_s) and normalized difference vegetation index (NDVI) to retrieve SSM using AMSR-E T_b. The SSM retrieval accuracy reaches $0.027 m^3/m^3$. Hong and Shin (2011) estimated the global SSM over land surface using a relation between the complex dielectric constant and SSM after retrieving the surface roughness and complex dielectric constant. SSM retrieval accuracy was about $0.06 m^3/m^3$. Li et al. (2011) used two-parameter retrieval approach (TWRA) and three-parameter retrieval approach (THRA) to retrieve global SSM. Both methods firstly simulated the surface roughness, vegetation and T_s condition and then retrieved SSM from AMSR-E T_b. The SSM retrieval accuracies were 0.089 and 0.037 m^3/m^3, respectively.

Former studies mainly focused on retrieving SSM information from simulated T_s, surface roughness and vegetation information (vegetation index, water content and optical depth). More recently, microwave polarization difference indices (MPDI) are proposed as a measure of differences in polarization signals and the soil dielectric properties (and therefore soil moisture). MPDI is also an effective indicator for characterizing the land surface vegetation cover condition (Paloscia et al. 1988; Wang et al. 2005). Based on land surface vegetation cover classification and land surface roughness classification, this paper presents a much simper semi-empirical relation among SSM, AMSR-E T_b, MPDI and T_s. With simple land surface roughness and vegetation classification only, SSM information can be retrieved from the semi-empirical model integrating

AMSR-E C-band T_b, MPDI, and T_s data for each land classification type. This SSM retrieval model also achieves a much higher accuracy under dense vegetation cover and rough surface covered situations than most former studies, which find it difficult to retrieve SSM information accurately under dense vegetation or rough surface areas.

2. Study Data and Area

2.1. Study area

Guangdong Province (gray region in Fig. 1a), a coastal province, located in southern China, with a population of 86,420,000 people and area of 177,900 km^2, is chosen as the study area. Climate here is the typical subtropical monsoon maritime climate of southern Asia, with an average annual sunshine of 1688.9 hours, an average temperature of 22.8℃ (23.2℃ in urban region). Since 2004, three disastrous droughts have occurred in Guangdong Province of southern China, which caused serious economic losses. In 2004-2005, the drought spread in Guangdong's 84 cities and counties, affecting more than 2 million residents (Fig. 1c). More than 689,000 hectares of farmlands were seriously affected. The economic losses from agriculture alone came to more than 1.4 billion Yuan (http://www.mwr.gov.cn/). In 2007, the amount of rainfall was about 60 % of normal year. Most cities even received less than 2,000 mm of rainfall. About 400,000 hectares of croplands were affected by drought, leading to total grain losses of 37.4 billion kg, causing 6.7 billion Yuan economic losses. In 2009, Guangdong Province had another unprecedented drought disaster. The average rainfall that year was 1,400 mm, 13 percent below normal years. This severe drought caused direct economic losses of 23.7 billion Yuan (http://www.chinadaily.com.cn). So, timely regional SSM information is useful for drought disaster monitoring, government decision-making and drought disaster prevention. To meet this

requirement to provide timely SSM information we have developed an improved SSM retrieval model using passive remote sensing data.

Insert Fig. 1 about here

2.2. Study data

The AMSR-E instrument on the NASA Earth Observing System (EOS) Aqua satellite is a modified version of the AMSR instrument launched on the Japanese Advanced Earth Observing Satellite-II (ADEOS-Ⅱ) in 1999. AMSR-E is a successor in technology to the Scanning Multi-channel Microwave Radiometer (SMMR) and Special Sensor Microwave Imager (SSM/I) instruments. It can provide global passive microwave measurements of terrestrial, oceanic, and atmospheric variables for the investigations of global water and energy cycles. Each AMSR-E T_b file contains images of six frequencies (6.9 GHz, 10.7 GHz, 18.7 GHz, 23.8 GHz, 36.5 GHz, and 89.0 GHz, Table 1). The instrument operated until October 4th, 2011, when AMSR-E reached its limit to maintain the rotation speed necessary for regular observations (40 rotations per minute), and the radiometer automatically halted its observations and rotations.

For this study we selected 4 days (October 28th &31st, 2004 and December 7th &8th, 2007) during the two drought disasters in 2004-2005 and 2007 to develop the SSM retrieval model, and used another 2 days (January 28th &31st, 2009) during the 2009 drought disaster to validate the SSM retrieval model. AMSR-E T_b data (version: AMSR-E/Aqua Daily EASE-Grid T_b) were downloaded from National Snow and Ice Data Center (NSIDC). Corresponding in-situ SSM and T_s were acquired from 86 meteorological observation stations (Fig. 1b) of Guangdong Province

(grey region in Fig. 1a). We also added the SSM mapping of another 5 days (April 1st, July 1st & December 31st, 2004 and April 1st & July 1st, 2005) in combination with October 31st 2004 to demonstrate the initiation, duration and recovery of the 2004-2005 severe drought disaster in Guangdong Province, southern China. A once-in-four-century heavy storm during June 18-25 caused an abrupt end to the 2004-2005 severe drought event.

Insert Table 1 about here

3. Methods

3.1 Developing the SSM retrieval model

The upwelling radiation from the land surface as observed from above the canopy may be expressed in terms of the radioactive brightness temperature T_{bp}, and can be given as a simple radioactive transfer equation (Owe et al., 2001):

$$T_{bp} = T_s * (1 - r_{sp}) e^{-\tau_c} + T_c (1 - w_p)(1 - e^{-\tau_c}) + r_{sp} T_c (1 - w_p)(1 - e^{-\tau_c}) e^{-\tau_c} \quad (1)$$

where p is the horizontal (H) or vertical (V) polarization mode; T_s represents the soil thermometric temperatures; r_{sp} is the smooth-surface reflectivity; τ_c is the optical depth of land surface vegetation; $e^{-\tau_c}$ is the transmissivity; T_c is thermometric temperatures of the canopy; w_p is the single scattering albedo. AMSR-E C channel is the low-frequency band, so this paper ignored the effects of single scattering albedo and atmosphere. Then, T_{bp} can be simplified as expression 2. If the texture of land surface can be seen as homogeneous, r_{sp} of the land surface can be seen as a constant, A_1.

$$T_{bp} = T_s * (1 - r_{sp}) e^{-2\tau_c} \quad (2)$$

According to Wang et al. (2006), τ_c can be simulated using an empirical function from MPDI and soil dielectric constant ε near land surface. The relative error of simulated τ_c is smaller than 5% compared with the simulation results of Owe et al. (2001):

$$\tau_c = -0.223 \ln \frac{MPDI}{\varepsilon^2} - 1.239^{0.12}\sqrt{MPDI - 0.001} + 0.00085\varepsilon^2 - 0.0547\varepsilon + 0.05411 \quad (3)$$

What is more, according to Dobson et al. (1985), ε can be expressed by body density of soil ρ_s, body density of solid materials ρ_r, SSM and the dielectric constant of pure water ε_{fw}.

$$\varepsilon = 1 + \frac{\rho_s}{\rho_r}(\varepsilon_r^{\eta} - 1) + SSM^{\beta}\varepsilon_{fw}^{\eta} - SSM \quad (4)$$

where η =0.06. If the soil texture of the study area is homogeneous, ρ_s, ρ_r, ε_r and ε_{fw} can be seen as constants, too. Thus, ε can be simplified as:

$$\varepsilon = A_2 + A_3 SSM^{A_4} - SSM \quad (5)$$

where A_2, A_3, A_4 are constants.

On assumption that the land surface can be seen as a homogeneous texture, we can establish a relation (expression 6) between SSM, T_s, MPDI and AMSR-E T_b from expression 2, 3 and 5.

$$\begin{aligned} &\ln A_1 - 0.892\ln(A_2 + A_3 SSM^{A_4} - SSM) - 0.0017(A_2 + A_3 SSM^{A_4} - SSM)^2 + 0.1096(A_2 + A_3 SSM^{A_4} - SSM) \\ &= \ln \frac{T_s - T_{bp}}{T_s} - 0.446\ln MPDI - 2.478^{0.12}\sqrt{MPDI - 0.001} + 0.10822 \end{aligned} \quad (6)$$

In summary, SSM can be easily retrieved using AMSR-E T_b, AMSR-E 6.9GHz MPDI and T_s for homogeneous land surface. The next step is to classify the land surface into several types according to different land surface vegetation cover condition and degree of surface roughness. Then, we assume that each land surface type is a homogeneous texture. So, expression 6 can be used to derive SSM for each land type.

3.2. Match AMSR-E T_b with in-situ data

The in-situ SSM and T_s observed by 86 meteorological observation stations were point-based.

In order to obtain the point-based AMSR-E T_b for each in-situ data, we averaged T_b of imagery-pixels around the 86 meteorological observation stations to match with the in-situ SSM and T_s. Firstly, AMSR-E T_b data was downloaded from ftp://n4ftl01u.ecs.nasa.gov. Then we extracted the latitude, longitude and T_b information and displayed the point-based T_b in ArcGIS software. About 2,223 pixels in total were extracted from each AMSR-E T_b file within Guangdong Province (black dots in Fig. 2). Then we drew 86 circles (radius: 9,000 m) centralized at each meteorological observation station (triangle points in Fig. 2) and averaged the pixels' T_b values within the circles to match with the SSM and T_s data from the meteorological observation stations.

Insert Fig. 2 about here

3.3. Land surface vegetation cover classification method

Chen et al. (2011) has established an empirical classification rule for land surface vegetation cover classification in Guangdong Province using AMSR-E MPDI values. Three land surface vegetation cover types were produced according to different AMSR-E MPDI values. For dense vegetation cover land surfaces, AMSR-E 6.9GHz MPDI is smaller than 0.06; For sparse vegetation cover regions, MPDI is between 0.06 and 0.09; For bare soil areas, MPDI value is generally larger than 0.09. The land surface vegetation cover classification method proved to be effective in T_s retrieval of Guangdong Province ($R^2 > 0.71$, $P < 0.05$).

3.4. Land surface roughness classification method

Surface roughness is another factor influencing SSM estimation. According to the empirical surface roughness model of Jin et al. (1998), the reflectivity of rough surface can be defined as:

$$r_{sv} = [(1-Q)r_{ov} + Qr_{oh}]e^{-h} \quad (7a)$$

$$r_{sh} = [(1-Q)r_{oh} + Qr_{ov}]e^{-h} \quad (7b)$$

where Q is a polarization mixing parameter, $0<Q<0.5$; h is the vertical surface roughness parameter; r_{sv} and r_{sh} represent the vertical polarization and horizontal polarization reflectivity of rough surface respectively; r_{ov} and r_{oh} indicate the vertical polarization and horizontal polarization reflectivity of flat surface respectively.

Combining the radiative brightness temperature (expression 2) and the reflectivity of rough surface (expression 7), MPDI can be expressed as (Ma, 2007):

$$\frac{1}{MPDI} = \frac{r_{ov} + r_{oh}}{(1-2Q)(r_{ov} - r_{oh})} - \frac{1}{(1-2Q)(r_{ov} - r_{oh})} 2e^{2\tau_c + h} \quad (8)$$

where $r_{ov} + r_{oh}$ and $(1- 2Q)(r_{ov} - r_{oh})$ are only influenced by SSM. Using MPDI from the AMSR-E 6.9GHz, 10.7GHz and 18.7GHz bands, Ma (2007) finally came to the following equation:

$$\Gamma = \frac{\frac{1}{MPDI_{6.9}} - \frac{1}{MPDI_{10.7}}}{\frac{1}{MPDI_{18.7}} - \frac{1}{MPDI_{10.7}}} = \frac{e_{6.9}{}^{2\tau_c + h} - e_{10.7}{}^{2\tau_c + h}}{e_{18.7}{}^{2\tau_c + h} - e_{10.7}{}^{2\tau_c + h}} \quad (9)$$

However, Γ is not only influenced by surface roughness condition, but also by vegetation cover condition. Thus, Γ can not be treated as a roughness index. This paper further assumes that τ_c of different AMSR-E bands has a linear relationship with each other ($e_{6.9}{}^{\tau_c} \approx \mathrm{m}\, e_{10.7}{}^{\tau_c} \approx \mathrm{n}\, e_{18.7}{}^{\tau_c}$, where m and n are constants). Then, expression 9 can be simplified as:

$$\frac{\frac{1}{MPDI_{6.9}} - \frac{1}{MPDI_{10.7}}}{(\frac{1}{MPDI_{18.7}} - \frac{1}{MPDI_{10.7}}) e_{6.9}{}^{2\tau_c}} = \frac{1-m}{n-m} * \frac{e_{6.9}{}^{h} - e_{10.7}{}^{h}}{e_{18.7}{}^{h} - e_{10.7}{}^{h}} \quad (10)$$

Combing this result with the optical depth τ_c simulated by Owe et al. (2001), we construct a modified roughness index Γ_{MPDI} (unit: cm).

$$\Gamma_{MPDI} \approx -3.21111 \times \frac{\frac{1}{MPDI_{10.7}} - \frac{1}{MPDI_{6.9}}}{\frac{1}{MPDI_{18.7}} - \frac{1}{MPDI_{10.7}}} \times (MPDI_{6.9} - 0.33280) + 0.00178 \quad (11)$$

We can see that Γ_{MPDI} is only influenced by surface roughness parameter (h). It is an more reasonable index for characterizing the land surface roughness degree than Γ. In order to validate the accuracy of the improved surface roughness index Γ_{MPDI}, three-day global land surface roughness mapping results (Fig.3) were produced from Γ_{MPDI} using AMSR-E/Aqua Daily Global Quarter-Degree Gridded T_b data on October 31st, 2004, December 8th, 2007 and January 31st, 2009. 5535 samples were selected to compare with the global surface roughness results mapped by Hong (2010), who used a unique approach to estimate the small-scale roughness with the global AMSR-E T_b data on April 1st, 2009. There was a strong linear relationship (Fig.4) between the surface roughness calculated by Γ_{MPDI} and the surface roughness simulated by Hong (2010). We further extracted the surface roughness condition of Guangdong Province (Fig.5) and used Γ_{MPDI} to classify Guangdong's land surface roughness condition.

Insert Fig. 3 about here

Insert Fig. 4 about here

Insert Fig. 5 about here

3.5. Data processing flow diagram

Land surface vegetation cover condition and land surface degree of roughness are two major factors influencing the SSM retrieval accuracy. Hence this paper classified the land surface of Guangdong Province into several types according to different land surface vegetation cover condition and degree of surface roughness. Further, we assumed each land surface type as a

homogeneous texture. Then, the algorithm containing SSM, T_s, MPDI and AMSR-E T_b (expression 6) can be used to derive SSM for each land type. The processing flow and methods are shown in Fig. 6.

Insert Fig. 6 about here

4. Results and Discussion

4.1 Land surface classification

On the basis of the land surface roughness mapping results (Fig. 7a), this paper further classified the land surface roughness of Guangdong Province into four types (Fig. 7b) using the land surface roughness classification rule in Table 2. Results showed that the surface roughness was lower in south and center of Guangdong Province, where most regions were river delta plain areas. It was much higher in north, east and northwest of Guangdong Province, where most regions were distributed by mountainous and hilly areas (Fig. 7b).

Considering that SSM can be influenced strongly by dense vegetations, this paper developed an improved vegetation classification method (Table 3) on the basis of Chen's empirical classification rule (Chen et al., 2011). Land surface vegetation cover classification results (Fig. 7c) showed that the land surface vegetation cover condition of Guangdong Province varied as latitude changed. Vegetation density at higher latitudes was much higher than vegetation density at lower latitudes (Fig. 7d). It was because that most regions at lower latitudes were close to sea and belonged to the built-up places, and most places at higher latitudes were mainly mountain areas or hilly grounds and were usually covered by dense broad-leaved forests, coniferous forests or

bushes.

Insert Table 2 about here

Insert Table 3 about here

Insert Fig. 7 about here

In combination with the land surface vegetation cover classification and land surface roughness classification results, 86 meteorological observation stations in Guangdong Province were classified into 5 types (Table 4 and Fig. 8). Then, each land surface type can be seen with a similar vegetation cover condition and surface roughness degree. In other words, each land type can be seen as a homogeneous land surface texture. Therefore, the SSM retrieval model (expression 6) can be used to retrieve the SSM information for each land type.

Insert Table 4 about here

Insert Fig. 8 about here

4.3. Surface soil moisture retrieval and validation

Using the land surface classification results of Guangdong Province and the SSM retrieval model (formula 6), this paper derived the SSM information for each land type separately from AMSR-E C-band T_b, MPDI and T_s. Levenberg-marquardt optimization algorithm (LMA) was used to solve the fitted coefficients (A1, A2, A3, A4) of SSM retrieval algorithm for each land type. As estimated by authors, the threshold value of A1 was between 0 and 1; the threshold value of A2

was larger than 10. Hence the original values of A1 and A2 were set as 0.5 and 11, respectively. The number of the optimization loops was set to 10. There were always single solutions for A1, A2, A3, A4 (Table 5) for each land type.

Insert Table 5 about here

In-situ measurements of SSM on January 28th & 31st, 2009 were used to validate the simulation accuracy of SSM (Fig.9a) from the corresponding ANSR-E data (N=86*2). Results showed that the average errors between in-situ and model-derived SSM values of the five algorithms were between 2.11% and 8.52%, with RMSE between 0.94% and 6.69% (Table 6, Fig. 9b). The total average SSM error was 5.37% with average RMSE equaling to 6.36% (R^2=0.87). The accuracy of the SSM retrieval result was higher than former studies (Wigneron et al., 2003; Uitdewilligen et al., 2003; Cashion et al., 2005; Bindlish et al. 2006; Loew et al., 2008; Panciera et al., 2009), of which the SSM retrieval accuracy was usually larger than 4%. Some former studies (Wigneron et al., 2003; Bindlish et al., 2006; Panciera et al., 2009) also found it difficult to retrieve SSM information accurately under dense vegetation or rough surface areas (SSM retrieval error in some studies even reached 32%). However, the SSM retrieval model developed in this paper achieved a much higher accuracy at 6.95% under dense vegetation cover (0.01<MPDI<0.06) and rough surface covered situations (roughness >0.3 cm). All the SSM retrieval errors were smaller than 20%. Results indicated that the semi-empirical SSM model can not only be applied to bare land areas and flat surface areas, but also to sparse vegetation covered areas, dense vegetation covered areas and rough surface areas.

Insert Table 6 about here

Insert Fig. 9 about here

The eight model-derived SSM maps and corresponding spatial-interpolated in-situ SSM maps from 86 meteorological observation stations on April 1st, July 1st, October 31st, & December 31st, 2004, April 1st & July 1st, 2005, December 8th, 2007 and January 31st, 2009 were presented in Fig.10. We can easily find that the initiation of the 2004-2005 drought disaster was on about July 1st, 2004, which should have lasted some days. The drought degree became more serious on October 31st, 2004. The most severe drought degree was about on December 31st, 2004. Then, it recovered a little on April 1st, 2005. There was nearly no drought condition in Guangdong on July 1st, 2005 because there was a synoptic process of heavy storm at once-in-four-century from June 18 to June 25, 2005 (http://news.gd.sina.com.cn/local/2005-12-31/2050082.html). The drought disaster lasted for almost one year. Time series of SSM mapping results during the 2004-2005 drought disaster indicated that the presented method was effective to detect the initiation, duration and recovery of a whole drought event.

Insert Fig. 10 about here

5. Conclusions

Three severe droughts have occurred in Guangdong Province of southern China during the past 10 years with disastrous consequences for the people of Guangdong. It is of great

importance to establish an effective SSM retrieval model using passive microwave remote sensing for monitoring the drought disasters. A simple SSM retrieval methodology derived from the passive microwave radiance transfer equation is presented in this study and proves to be effective in retrieving SSM information using AMSR-E C-band T_b, MPDI and T_s.

Land surface vegetation cover condition and degree of roughness are two major factors influencing the SSM accuracy retrieval from AMSR-E T_b. This paper uses MPDI to characterize the vegetation cover condition of Guangdong Province, and develops a modified surface roughness index to map the surface roughness condition of Guangdong Province, which was validated at the global scale. Results show that land surface vegetation density of Guangdong is always higher at higher latitudes than at lower latitudes. Surface roughness is lower in south and central of Guangdong Province, while much rougher in north, east and southwest. Furthermore, this study classifies the land surface into five types according to different vegetation cover and surface roughness condition and then assumes each land surface type having a homogeneous land surface texture.

A simple semi-empirical SSM retrieval model is developed for each land surface type with much higher retrieval accuracy. Validation results from three different drought cases prove that it is an effective way to derive SSM information and monitor the degree of drought condition from AMSR-E T_b data (average SSM error is 5.37%: R^2=0.87, RMSE=6.36%). All the SSM retrieval errors are smaller than 20%. What is more, the average SSM retrieval error is under 6.95% for dense vegetation cover (0.01<MPDI<0.06) and rough surface cover condition (roughness>0.3cm), which is also smaller than most former studies (Wigneron et al., 2003; Bindlish et al. 2006; Panciera et al., 2009). The semi-empirical SSM retrieval model can not only be applied to bare

ground and flat surface areas, but also to sparse vegetation covered areas, dense vegetation cover areas and rough surface areas. Time series of SSM retrievals from AMSR-E imageries indicate that the 2004-2005 drought event lasted more than one year from April 1st, 2004 to July 1st, 2005. Hence the method presented here was effective to detect the initiation, duration and recovery of drought disasters.

Acknowledgement

This study was supported jointly by the National Basic Research Program of China (973 Program) (Grant No. 2011CB707103), National Natural Science Foundation of China (NO.40701127), Science and Technology Plan Fund of Guangdong Province, China (2010B020315016, 2010B020315029 & 2007B020500002-7).

References

Bindlish R., Jackson T.J., Gasiewski A.J., Klein M., & Njoku E.G. (2006). Soil moisture mapping and AMSR-E validation using the PSR in SMEX02. *Remote Sensing of Environment*, 103, 127–139.

Cashion J., Lakshmi V., Bosch D., & Jackson T. (2005). Microwave remote sensing of soil moisture: evaluation of the TRMM microwave imager (TMI) satellite for the Little River Watershed Tifton, Georgia. *Journal of Hydrology*, 307, 242–253.

Chanzy A., & Wigneron J.P. (2000). Microwave emission from soil and vegetation. Matzler, C. (Ed), EUR 19543—COST Action 712— Radiative Transfer Models for Microwave Radiometry. Office for Official Publications of the European Communities, Luxembourg, for European Commission, p. 174.

Chen S.S., Chen X.Z., Chen W.Q., Su Y.X., & Li D. (2011). A simple retrieval method of land surface temperature from AMSR-E passive microwave Data – A case Study over southern China during the strong snow disaster of 2008. International *Journal of Applied Earth Observation and Geoinformation*, 13, 140–151.

Choudhury B.J. (1987). Relationships between vegetation indices, radiation absorption, and net photosynthesis evaluated by a sensitivity analysis. *Remote Sensing of Environment*, 22, 209–233.

Choudhury B.J., Schmugge T.J., & Mo T. (1982). A parameterization of effective soil temperature for microwave emission. *Journal of Geophysical Research*, 87 (C2), 1301–1304.

Dobson M.C., Ulaby F.T., Hallikainen M.T., & El-Rayes M.A. (1985). Microwave dielectric behaviour of wet soil—part II: dielectric mixing models. *IEEE Transactions on Geoscience & Remote Sensing*, 23 (1), 35–46.

Eagleman J.R., & Lin W.C. (1976). Remote sensing of soil moisture by a 21-cm passive radiometer. *Journal of Geophysical Research*, 81(21), 3660–3666.

Hallikainen M.T., Ulaby F.T., Dobson M.C., El-Rayes M.A., & Wu L. (1985). Microwave dielectric behaviour of wet soil—part I: empirical models and experimental observations. *IEEE Transactions on Geoscience & Remote Sensing*, 23 (1), 25–34.

Hong S. (2010). Global retrieval of small-scale roughness over land surfaces at microwave frequency. *Journal of Hydrology*, 389, 121–126.

Hong S., & Shin, I. (2011). A physically-based inversion algorithm for retrieving soil moisture in passive microwave remote sensing. *Journal of Hydrology*, 405, 24-30.

Jackson T.J., & Schmugge T.J. (1989). Passive microwave remote sensing system for soil moisture:

Some supporting research. *IEEE Transactions on Geoscience & Remote Sensing*, 27 (2), 225–235.

Jackson T.J., Le Vine D.M., Hsu A.Y., Oldak A., Starks P.J., Swift C.T., Isham J.D., & Haken M. (1999). Soil moisture mapping at regional scales using microwave radiometry: the Southern Great Plains hydrology experiment. *IEEE Transactions on Geoscience & Remote Sensing*, 37(5), 2136–2151.

Jackson T.J., Le Vine D.M., Swift C.T., Schmugge T.J., & Schiebe F.R. (1995). Large area mapping of soil moisture using the ESTAR passive microwave radiometer in Washita '92. *Remote Sensing of Environment*, 53, 27–37.

Jackson T.J., O'Neill P.E., & Swift C.T. (1997). Passive microwave observation of diurnal surface soil moisture. *IEEE Transactions on Geoscience & Remote Sensing*, 35(5), 1210–1222.

Jin Y.Q. (1998). Monitoring regional sea ice of China's bo hai sea by using SSM/I scattering indexes. *IEEE Journal of Oceanic Engineering*, 23(2),141-144.

Lacava T., Cuomo V., Di Leo E. V., Pergola N., Romano F., &Tramutoli V. (2005). Improving soil wetness variations monitoring from passive microwave satellite data: The case of April 2000 Hungary flood. *Remote Sensing of Environment*, 96 , 135 – 148.

Li Q., Zhong R. F., Huang J. X., Gong H. L. (2011). Comparison of two retrieval methods with combined passive and active microwave remote sensing observations for soil moisture. *Mathematical and Computer Modelling*, 54, 1181-1193.

Liebe H.J. (1989). MPM—an atmospheric millimeter-wave propagation model. *International Journal of Infrared Millimeter Waves*, 10, 631–650.

Loew A. (2008). Impact of surface heterogeneity on surface soil moisture retrievals from passive

microwave data at the regional scale: The Upper Danube case. *Remote Sensing of Environment*, 112, 231–248.

Ma Y. (2007). Study on soil moisture inversion and application with microwave remote sensing in Xinjiang. *Xnjiang University*, Xinjiang, 45-75.

Mallick K., Bhattacharya B. K., Patel N.K. (2009). Estimating volumetric surface moisture content for cropped soils using a soil wetness index based on surface temperature and NDVI. *Agricultural and Forest Meteorology*, 149, 1327-1342.

Owe M., De Jeu R., Holmes T. (2008). Multi-sensor historical climatology of satellite derived global land surface moisture. *Journal of Geophysical Research*,113, F01002. doi:10.1029/2007JF000769.

Owe M., Jeu R.D., & Walker J. (2001). A methodology for surface soil moisture and vegetation optical depth retrieval using the Microwave Polarization Difference Index. *IEEE Transactions on Geoscience & Remote Sensing*, 39(8), 1643-1654.

Paloscia S., & Pampaloni P. (1988). Microwave Polarization Index for Monitoring Vegetation Growth. *IEEE Transactions on Geoscience & Remote Sensing*, 26(5), 617-621.

Panciera R., Walker J.P., Kalma J.D., Kim E.J., Saleh K., & Wigneron J.P. (2009). Evaluation of the SMOS L-MEB passive microwave soil moisture retrieval algorithm. *Remote Sensing of Environment*, 113 (2009), 435–444.

Schmugge T.J., & Jackson T.J. (1992). A dielectric model of the vegetation effects on the microwave emission from soils. *IEEE Transactions on Geoscience & Remote Sensing*, 30 (4), 757–760.

Schmugge T.J., (1998). Applications of passive microwave observations of surface soil moisture.

Journal of Hydrology, 3(5), 188–197.

Schmugge T.J., Wang J.R., & Asrar G. (1988). Results from the push broom microwave radiometer flights over the Konza Prairie in 1985. *IEEE Transactions on Geoscience & Remote Sensing*, 26(5), 590–596.

Uitdewilligen D.C.A., Kustas W.P. , & van Oevelen P.J. (2003). Estimating surface soil moisture with the scanning low frequency microwave radiometer (SLFMR) during the Southern Great Plains 1997 (SGP97) hydrology experiment. *Physics and Chemistry of the Earth*, 28, 41–51.

Ulaby F.T., Moore R.K., Fung A.K. (1982). Microwave Remote Sensing: Active and Passive, vol. 2. Artech House, Boston.

Wang J.R., Shiue J.C., Schmugge T.J., & Engman E.T. (1990). The Lband PBMR measurements of surface soil moisture in FIFE. *IEEE Transactions on Geoscience & Remote Sensing*, 28(5), 906–914.

Wang J.R., Shiue J.D., Schmugge T.J., & Engman E.T. (1989). Mapping surface soil moisture with L-band radiometric measurements. *Remote Sensing of Environment*, 27, 305–312.

Wang L., Li Z., & Chen Q. (2006). The Applications of MPDI during the Soil Moisture Retrieval from Radiometer in the Region with Vegetation Cover. *Journal of Remote Sensing*, 10(1), 34-38.

Wigneron J.P., Calvet J.C., Pellarin T., Van de Griend A.A., Berger M., & Ferrazzoli P. (2003). Retrieving near-surface soil moisture from microwave radiometric observations: current status and future plans. *Remote Sensing of Environment*, 85, 489–506.

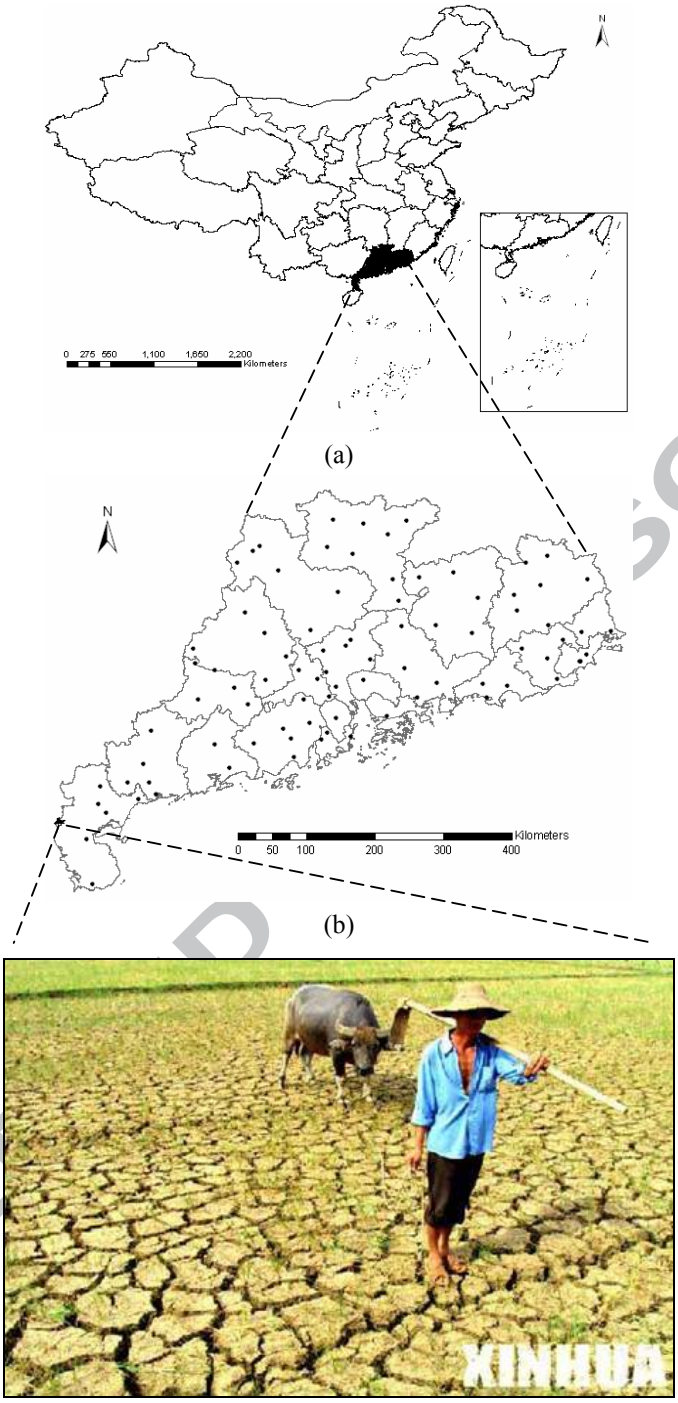

Fig.1 The location of study area: (a) Location of Guangdong Province in China (shadow area); (b) Eighty-six meteorological observation stations (black circle points) in Guangdong; (c) The scene of drought disaster in Lemin Town of Zhanjiang city of Guangdong Province on June 5th, 2005 during the severe drought of 2004-2005.

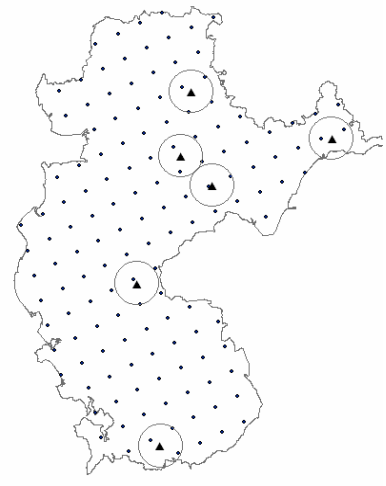

Fig.2 The matching method of remote sensing pixel to ground observation of SSM: the T_b values of circle-included pixels (dots) from AMSR-E data were averaged to match with the in-situ SSM data from the 86 meteorological observation stations (triangles) in Guangdong Province (circle radius: 9,000m) .

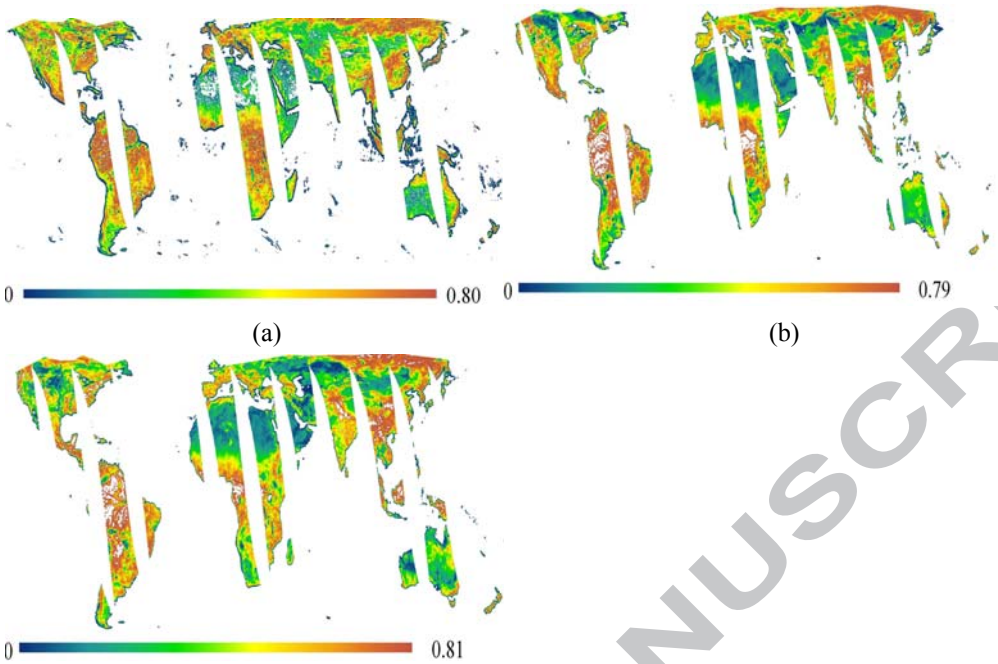

Fig.3 Mapping of global land surface roughness on (a) October 31st, 2004, (b) December 8th, 2007 and (c) January 31st, 2009 using the modified surface roughness index Γ_{MPDI} (unit: cm).

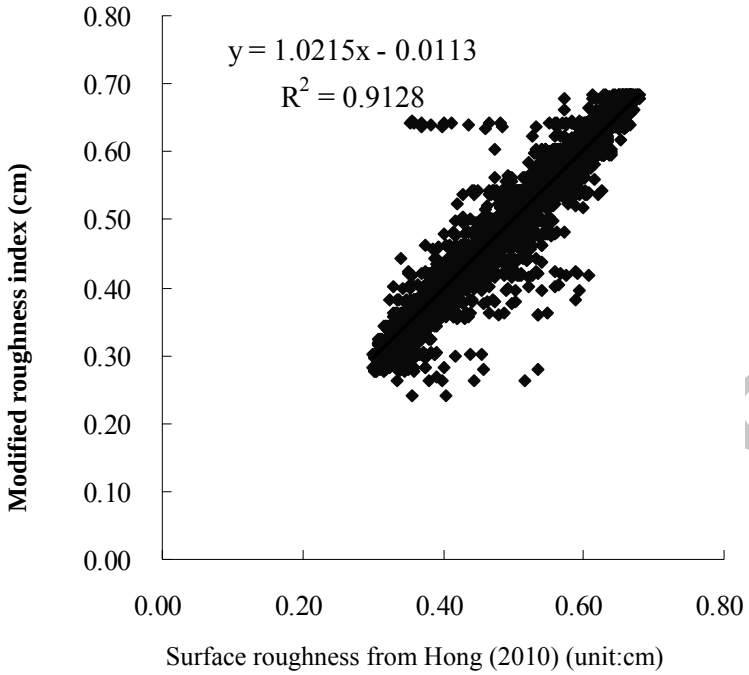

Fig.4 Comparison between the surface roughness simulated using the modified roughness index (Γ_{MPDI}) in the study and the surface roughness calculated by Hong (2010), using AMSR-E/Aqua Daily Global Quarter-Degree Gridded T_b data on October 31st, 2004, December 8th, 2007 and January 31st, 2009.

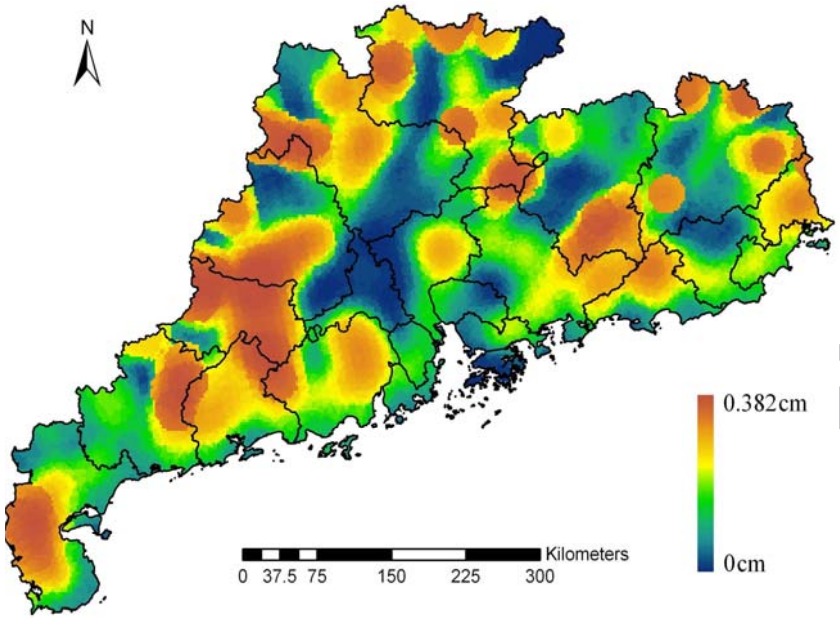

Fig.5 Land surface roughness condition of Guangdong Province on October 31st, 2004 derived from the modified surface roughness index (Γ_{MPDI}).

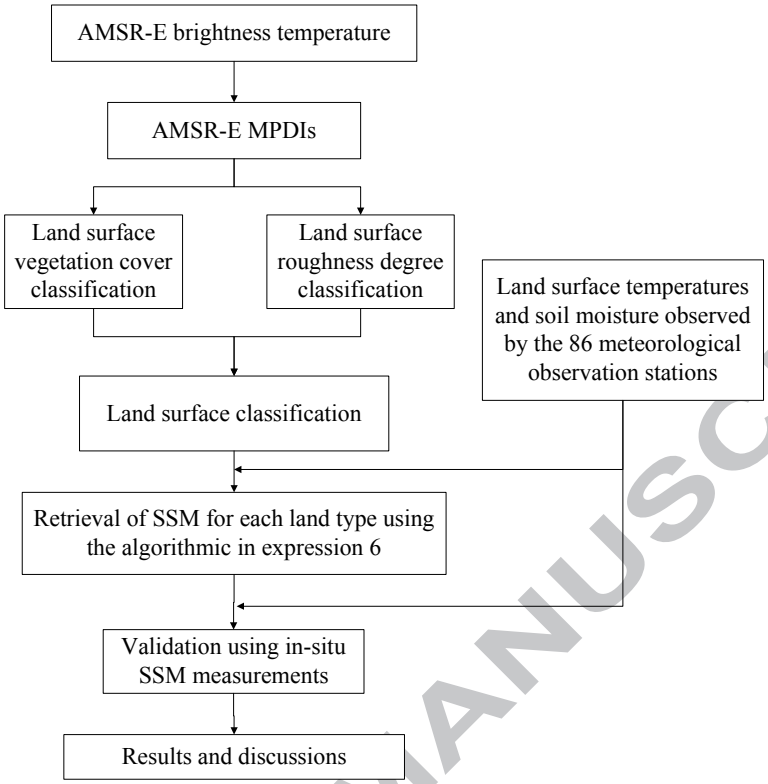

Fig. 6 Data processing flow diagram for mapping SSM from AMSR-E T_b data.

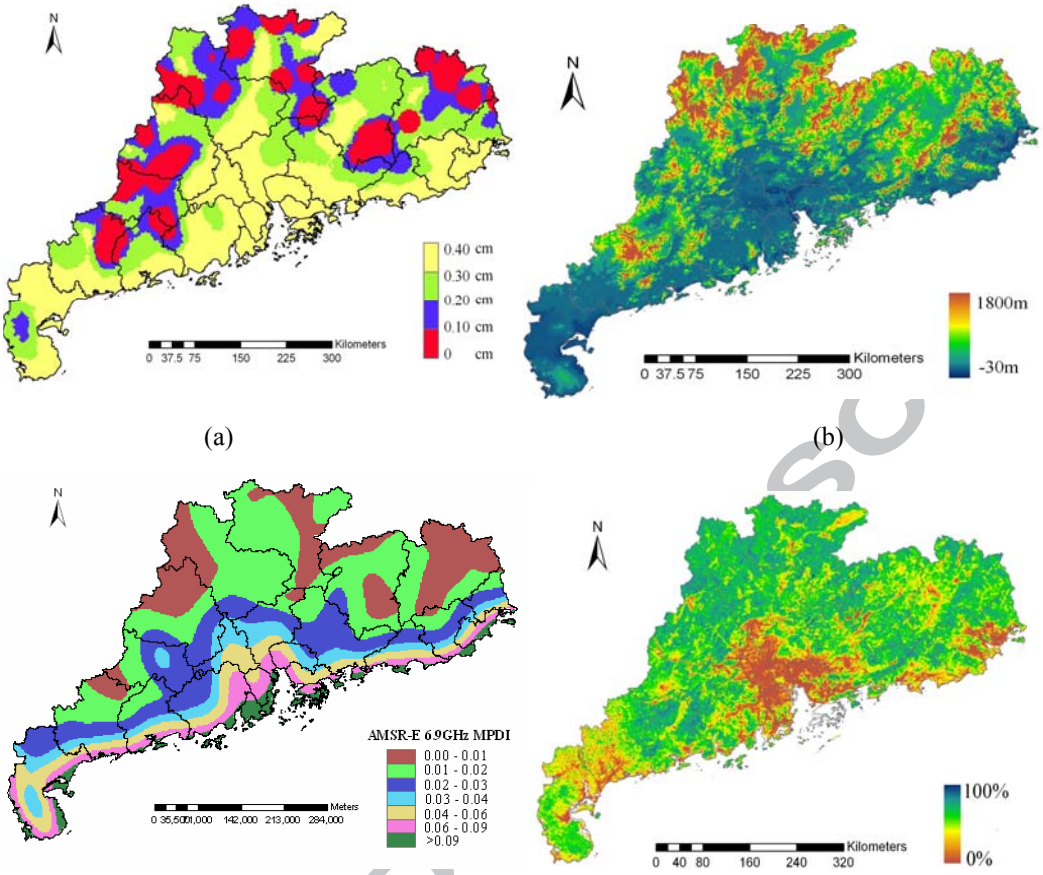

Fig. 7 (a) Land surface roughness classification results of Guangdong Province; (b) Elevation map of Guangdong Province in 2005; (c) MPDI-based Land surface vegetation cover classification results of Guangdong Province; (d) Vegetation coverage map of Guangdong Province in 2008.

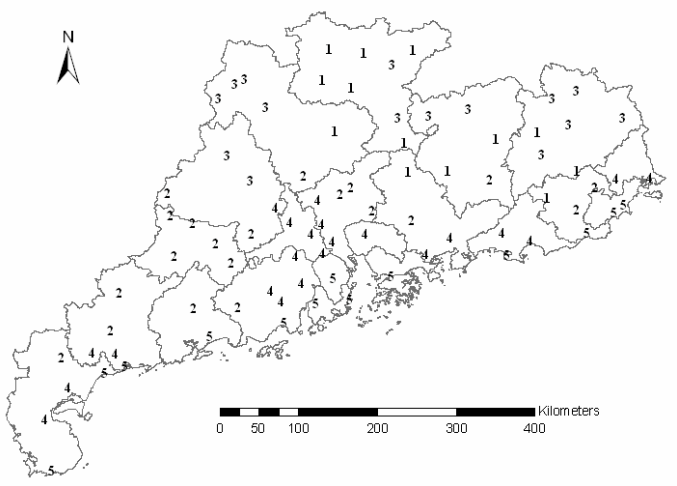

Fig. 8 Vegetation cover- and roughness-based land surface types of the 86 meteorological observation stations in Guangdong Province. Different numbers represent different land surface types (1: type 1, 2: type 2, 3: type 3, 4: type 4, 5: type 5). The positions of the numbers indicate the positions of the 86 meteorological observation stations.

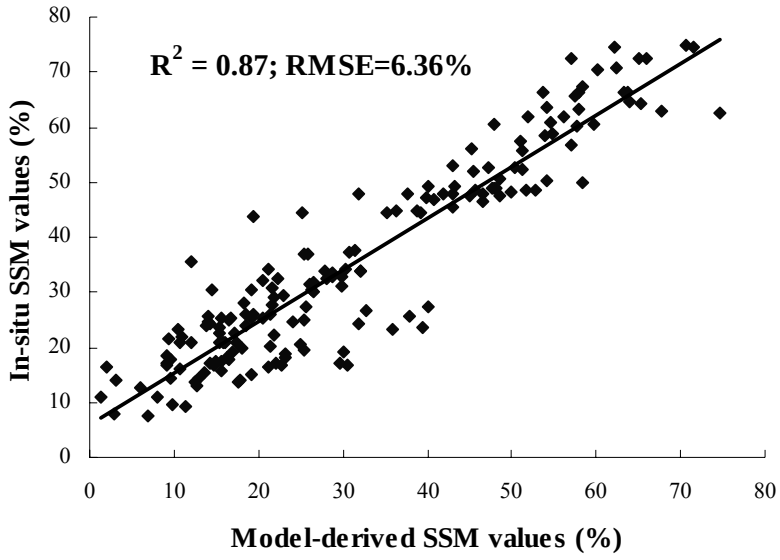

(a)

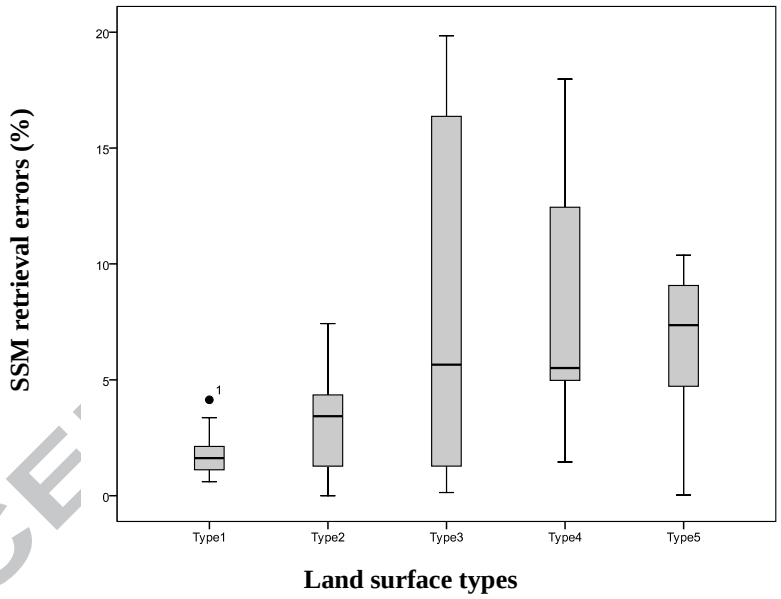

(b)

Fig. 9 Validation of SSM inversion: (a) Scatter diagram between in-situ and model-derived SSM on January 28th &31st, 2009 (N=2*86); (b) Error boxplot between in-situ SSM and model-derived SSM for each land surface type. The maximum of the error bar represents the biggest error between in-situ and model-derived SSM; the minimum of the error bar represents the smallest error between in-situ and model-derived SSM; the center of the error bar represents the average error between in-situ and model-derived SSM.

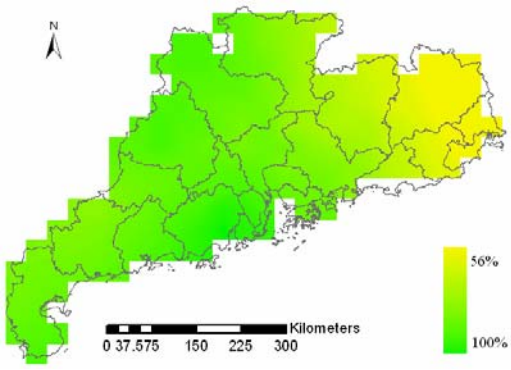

(a1)Model-derived SSM on April 1st, 2004

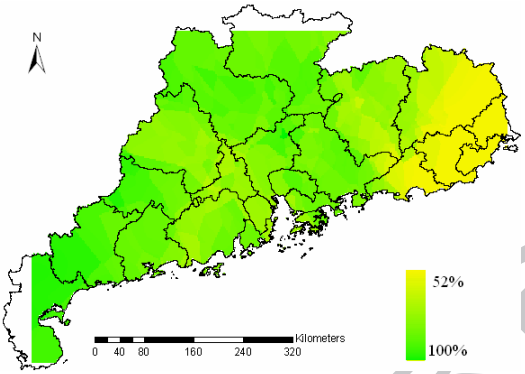

(a2)In-situ SSM on April 1st, 2004

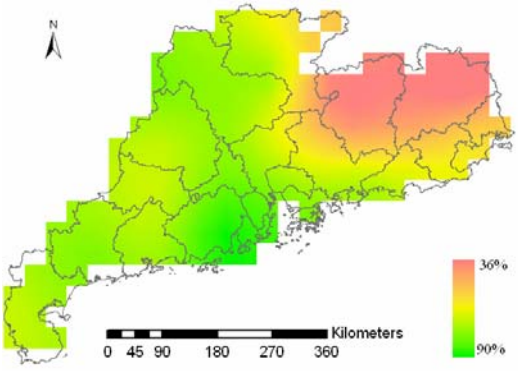

(a3)Model-derived SSM on July 1st, 2004

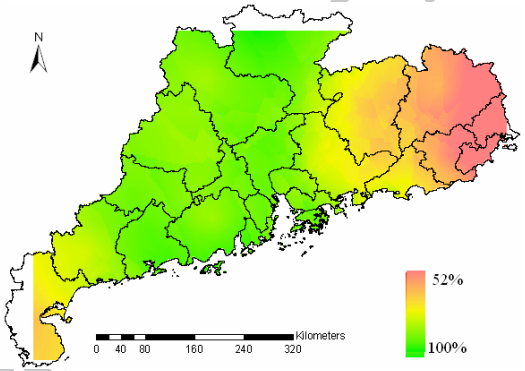

(a4)In-situ SSM on July 1st, 2004

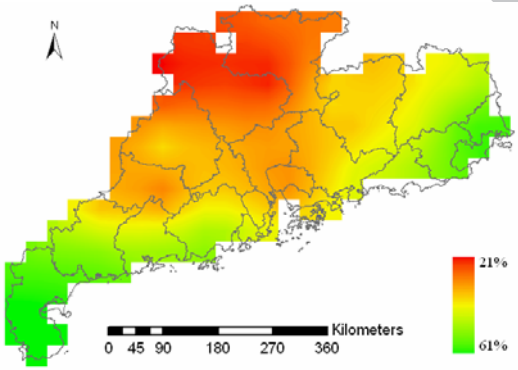

(a5)Model-derived SSM on Oct 31st, 2004

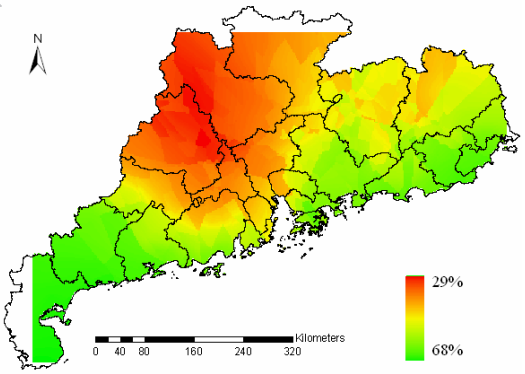

(a6)In-situ SSM on Oct 31st, 2004

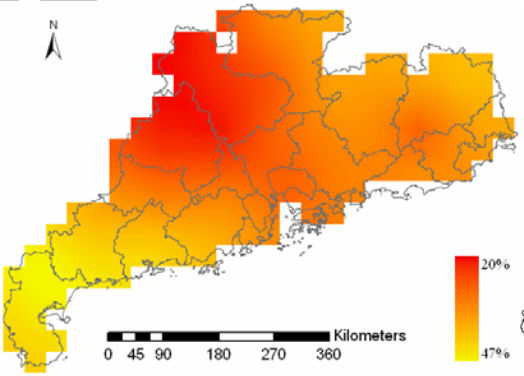

(a7)Model-derived SSM on Dec 31st, 2004

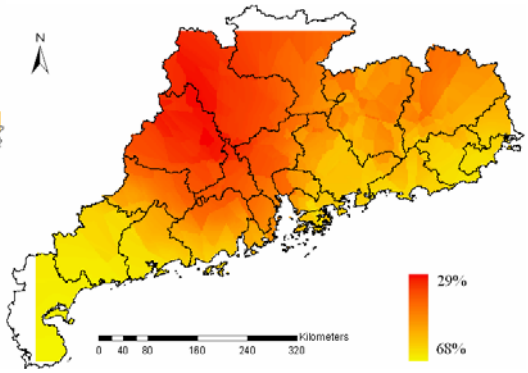

(a8)In-situ SSM on Dec 31st, 2004

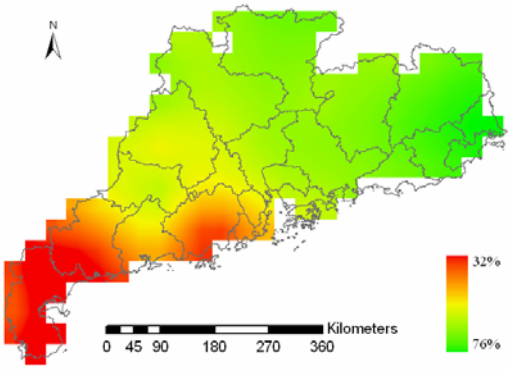

(a9)Model-derived SSM on April 1st, 2005

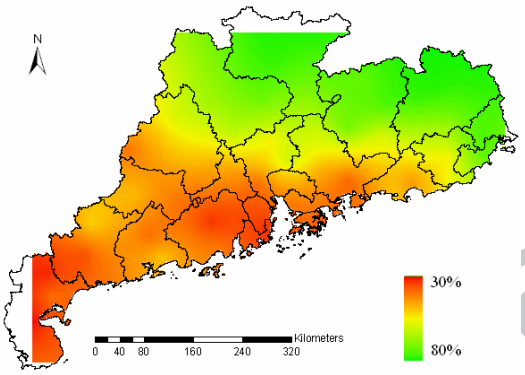

(a10)In-situ SSM on April 1st, 2005

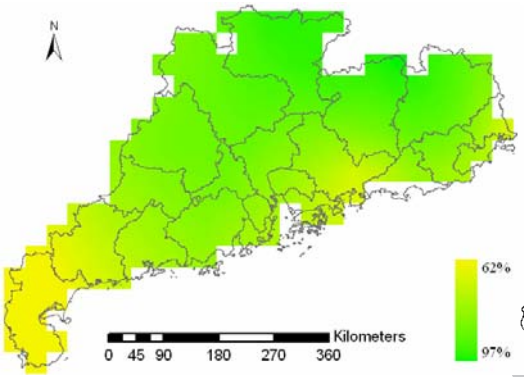

(a11)Model-derived SSM on July 1st, 2005

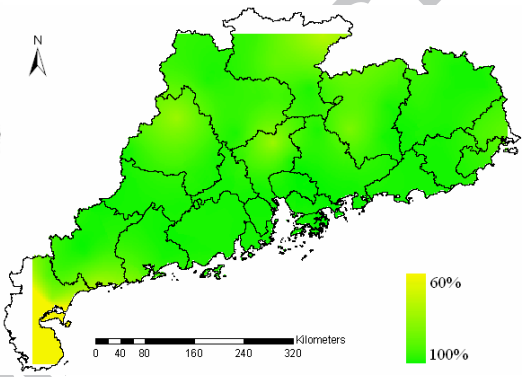

(a12)In-situ SSM on July 1st, 2005

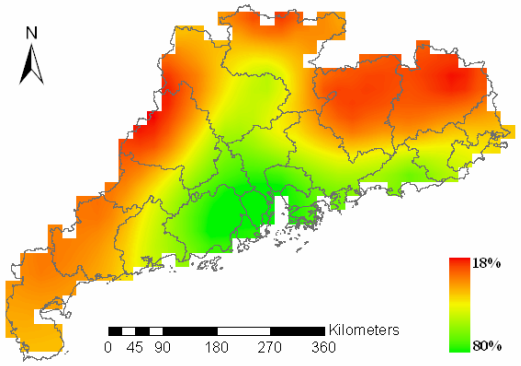

(a13)Model-derived SSM on Dec 8th, 2007

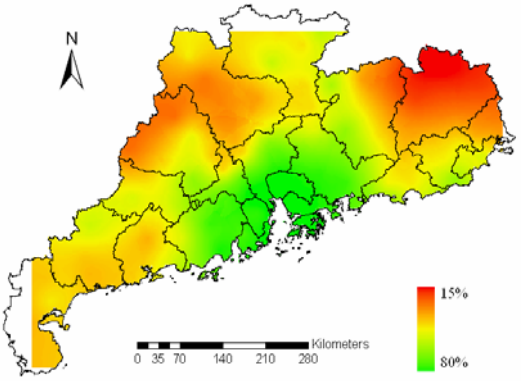

(a14)In-situ SSM on Dec 8th, 2007

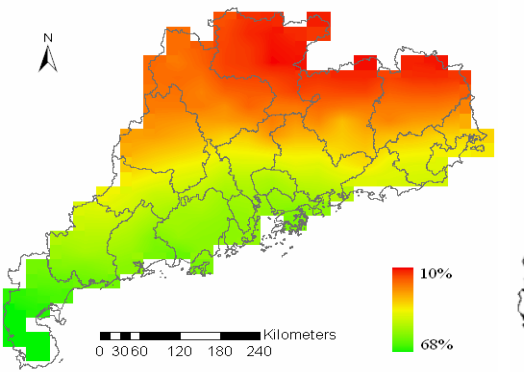

(a15)Model-derived SSM on Jan 31st, 2009

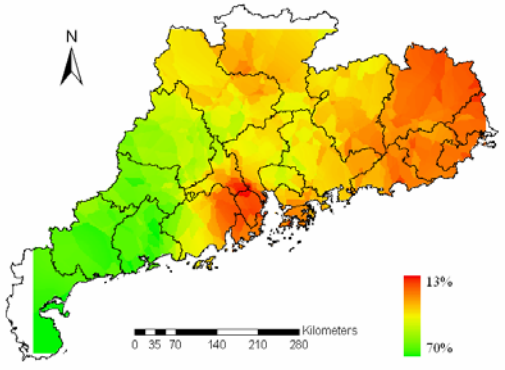

(a16)In-situ SSM on Jan31st, 2009

Fig. 10 Mapping of the model-derived SSM and in-situ SSM in Guangdong Province including the initiation, duration and recovery for the disastrous drought event of 2004-2005 (a1-a12). The severe droughts of years 2007 and 2009 in Guangdong Province were spatially mapped in a13-a16.

Table 1 Spatial characteristic of AMSR-E brightness temperature products.

Footprint Size	Mean spatial resolution	Channels (GHz)					
		89.0	36.5	23.8	18.7	10.7	6.9
75km * 43km	56 km	△	△	△	△	△	△
51km * 29km	38 km	△	△	△	△	△	
27km * 16km	21 km	△	△	△			
14km * 8km	12 km	△					

△ means including the corresponding AMSR-E channel.

Table 2 Land surface roughness classification rule.

Γ_{MPDI} value	Land surface roughness types
0.0 - 0.1	flat
0.1 - 0.2	less flat
0.2 – 0.3	less rough
>0.30	rough

Table 3 Land surface vegetation cover classification rule.

AMSR-E 6.9GHz MPDI value	Land surface vegetation cover types
0.00-0.01	dense vegetationⅠ
0.01-0.02	dense vegetationⅡ
0.02-0.03	dense vegetation Ⅲ
0.02-0.04	dense vegetation Ⅳ
0.04-0.06	dense vegetation Ⅴ
0.06-0.09	sparse vegetation
>0.09	bare soil area

Table 4 Land surface types of the 86 meteorological observation stations.

Number	Land surface types
1	bare ground & flat
2	sparse vegetation & flat
3	sparse vegetation & rough
4	dense vegetation & less flat
5	dense vegetation & rough

Table 5 Regression coefficients of the SSM retrieval algorithm for each land surface type.

Land surface type	A1	A2	A3	A4	R^2
1	0.2109	17.9657	0.0407	1.8675	0.87
2	0.1944	18.0755	0.0410	2.1593	0.85
3	0.1375	16.8792	2.3566	1.2871	0.83
4	0.1511	13.1687	0.0204	2.4673	0.80
5	0.0915	28.4136	1.4641	4.1881	0.81

1 **Table 6** Errors between in-situ and model-derived SSM for each land surface type.

Land surface type	Average errors between in-situ SSM and derived SSM (%)	RMSE (%)
1	2.11	0.94
2	2.89	1.91
3	6.24	6.69
4	6.95	2.56
5	8.52	5.16

2

Research Highlights

1. The land surface was classified into five types based on different vegetation and roughness condition.
2. Improving a roughness index using three channels of AMSR-E T_b.
3. Developing a SSM model integrating T_b, MPDI and observed temperature data.
4. Inversed results discriminated over a broad range of SSM (7%~73%, RMSE: 6.36%).
5. The errors for dense vegetation and rough surfaces were smaller than former studies.
6. The method was effective to detect the initiation, duration and recovery of drought events.